4.2 W/mm at 10 GHz in Silicon Delta-Doped AlN/GaN/AlN Pseudomorphic HEMTs With PECVD SiN Passivation

Eungkyun Kim, Yu-Hsin Chen, Keisuke Shinohara, *Senior Member, IEEE*, Thai-Son Nguyen, Jimy Encomendero, Debdeep Jena, *Fellow, IEEE*, and Huili G. Xing, *Fellow, IEEE*

***Abstract*— We demonstrate AlN/GaN/AlN pseudomorphic high electron mobility transistors (pHEMTs) on bulk AlN substrates with silicon δ-doping near the bottom of the 20-nm GaN channel. Our recent studies on epitaxy and low-field transport show that δ-doping in pseudomorphic AlN/GaN/AlN heterostructures increases electron mobility and two-dimensional electron gas density while preserving the advantages of the thin GaN channel, compared to undoped counterparts. In this work, we present DC and RF characteristics of these pHEMTs with PECVD SiN passivation, exhibiting an average $f_T \cdot L_G$ product of 12.5 GHz·μm, a representative output power density of 4.2 W/mm with an associated power-added efficiency of 41.5% at 10 GHz.**

***Index Terms*— AlN, GaN, HEMT, RF, power.**

I. Introduction

DOUBLE-HETEROSTRUCTURE GaN-channel HEMTs (DH-HEMTs) have gained considerable attention over the years for high-power RF applications. The Al(Ga)N back barrier in DH-HEMTs, with its larger energy band gap, offers superior electron confinement, higher buffer electrical resistivity, and enhanced breakdown voltage compared to the conventional AlGaN/GaN single-heterostructures. Taking advantage of these improvements, superior performance of DH-HEMTs with an AlGaN back barrier have been demonstrated [1], [2], [3]. However, the inclusion of an AlGaN back barrier presents several challenges. First, AlGaN exhibits significantly lower thermal conductivity compared to GaN or AlN [4], [5]. The presence of high thermal resistance beneath the channel raises the channel temperature, thereby reducing device reliability and efficiency [6], [7]. Second, for epitaxial layers thicker than the pseudomorphic limit, lattice mismatch leads to a high density of threading dislocations and thermal boundary resistance, even with the use of free-standing bulk GaN or AlN substrates [8], [9].

To enhance device-level thermal management, pseudomorphic HEMTs (pHEMTs) on the AlN platform have been previously introduced [10], [11], [12], [13], [14], [15]. In this structure, a thin, coherently strained GaN channel is sandwiched between high thermal conductivity, ultra-wide bandgap AlN. When pHEMTs are grown on single-crystal AlN substrates, the dislocation density in the heterostructure can be minimized (limited by the dislocation density in the substrates), as the thin GaN channel layer is coherently strained on the underlying AlN back barrier, which is homoepitaxially grown on the single-crystal AlN substrates. Furthermore, homoepitaxy of AlN back barrier can eliminate thermal boundary resistance at the back barrier-substrate growth interface [16]. Combined with the high thermal conductivity of AlN ($\kappa \sim 340$ W/m·K), heat dissipation in pHEMTs on AlN can be significantly improved over conventional GaN HEMTs.

However, undoped pseudomorphic AlN/GaN/AlN heterostructures have exhibited electron mobility limited to $\mu \sim 600$ cm^2/V·s due to the high electric field in the GaN channel layer [17]. In our recent study, we showed that inserting compensation δ-doping near the bottom of the GaN channel can address this challenge while preserving good crystal quality, resulting in increased electron mobility and, consequently, lower sheet resistance [18]. Here, we demonstrate the DC and RF characteristics of HEMTs fabricated on this silicon δ-doped, pseudomorphic AlN/GaN/AlN heterostructure.

II. Epitaxial Growth and Device Design

The HEMT epitaxial heterostructure was grown by molecular beam epitaxy (MBE) (Fig. 1(a)), consisting of a 500 nm AlN buffer layer homoepitaxially grown on single-crystal AlN substrates from Asahi-Kasei Corporation [19], followed by a 20 nm coherently strained GaN channel and a 6 nm AlN top barrier capped with a 1 nm thick GaN layer. Silicon δ-doping

Received 22 July 2025; accepted 3 August 2025. Date of publication 6 August 2025; date of current version 29 September 2025. This work was supported in part by Army Research Office (ARO) under Grant W911NF-22-2-0177, in part by the Defense Advanced Research Projects Agency (DARPA) THREADS Program, in part by the Semiconductor Research Corporation (SRC) (SUPREME), in part by NORDTECH NITRIDER—Microelectronics Commons Program, a DoD initiative, under Grant N00164-23-9-G061, and in part by the Performed at the Cornell Nanoscale Facility, a National Nanotechnology Coordinated Infrastructure (NNCI) member supported by National Science Foundation (NSF) under Grant NNCI-2025233. The review of this letter was arranged by Editor J. Joh. *(Corresponding author: Eungkyun Kim.)*

Eungkyun Kim is with the School of Electrical and Computer Engineering, Cornell University, Ithaca, NY 14853 USA, and also with the Kavli Institue of Nanoscience, Cornell University, Ithaca, NY 14853 USA (e-mail: ek543@cornell.edu).

Yu-Hsin Chen and Thai-Son Nguyen are with the Department of Materials Science and Engineering, Cornell University, Ithaca, NY 14850 USA.

Keisuke Shinohara is with the Teledyne Scientific and Imaging, Thousand Oaks, CA 91360, USA.

Jimy Encomendero is with the School of Electrical and Computer Engineering, Cornell University, Ithaca, NY 14853 USA.

Debdeep Jena and Huili G. Xing are with the School of Electrical and Computer Engineering, the Department of Materials Science and Engineering, and the Kavli Institute of Nanoscience, Cornell University, Ithaca, NY 14853 USA.

Digital Object Identifier 10.1109/LED.2025.3596445

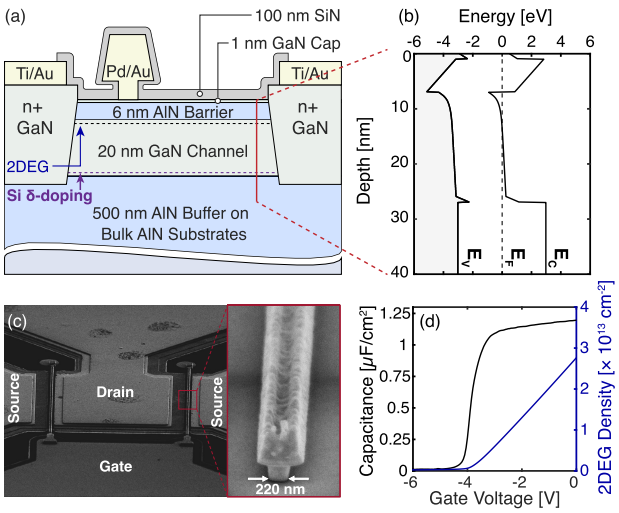

Fig. 1. (a) Cross-sectional representation of the fully processed silicon δ-doped pHEMT on bulk AlN and (b) simulated energy band diagrams. (c) SEM images of a fully processed device with two gate fingers with a 220 nm T-gate. (d) Capacitance-voltage characteristics (black) and extracted 2DEG density under the gate (blue).

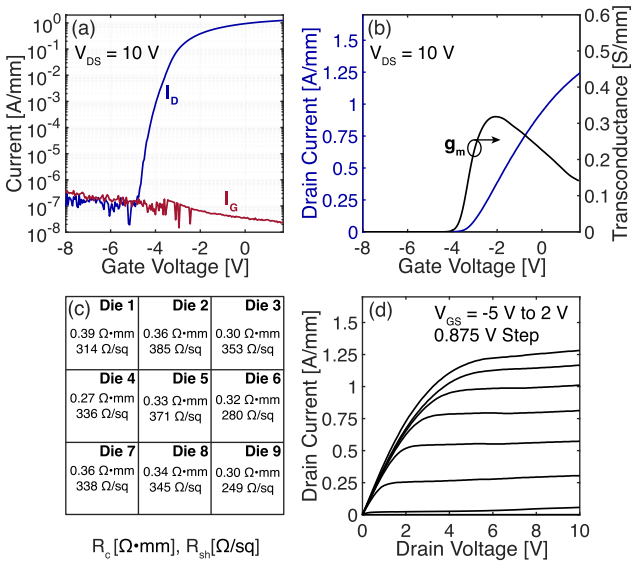

Fig. 2. Transfer characteristics in (a) logarithmic scale and (b) linear scale of unpassivated δ-doped pHEMTs on bulk AlN, showing a peak extrinsic transconductance of 0.32 S/mm and an on/off ratio spanning 7 orders of magnitude. (c) Die map of contact resistance and sheet resistance extracted from linear TLM patterns across nine dies on the sample. (d) output characteristics of unpassivated δ-doped pHEMTs, showing a maximum drain current density of 1.25 A/mm.

was inserted 1 nm above the bottom GaN/AlN interface. The coherency of the 20 nm GaN layer was confirmed by the reciprocal space mapping around the asymmetric (−105) diffraction peak, revealing −2.4% compressive strain in GaN on single-crystal AlN, which corresponds to the lattice mismatch between GaN and AlN. Detailed studies on epitaxy are summarized in [18]. Fig. 1(b) shows the simulated energy band diagram, illustrating the reduced electric field in the GaN channel as indicated by the slope of the conduction band. Hall-effect measurements performed on the as-grown heterostructure at room temperature revealed a 2DEG density of 2.77 × 10^{13} cm^{-2} and electron mobility of 690 $cm^2/V{\cdot}s$. For a more recently grown sample, a 2DEG density of 3.24 × 10^{13} cm^{-2} and an electron mobility of 855 $cm^2/V{\cdot}s$ were measured (devices not yet fabricated) [18].

The device fabrication process includes n^+ GaN regrowth for ohmic contact formation, device isolation using BCl_3-based inductively coupled plasma etching, Ti/Au non-alloyed ohmic metallization, electron-beam lithography-defined Pd/Au T-gate formation via electron-beam evaporation, and final device passivation with plasma-enhanced chemical vapor deposition (PECVD) SiN. Scanning electron microscope (SEM) images of a fully processed device are shown in Fig. 1(c). Unless otherwise specified, all measured devices feature a source-to-drain spacing $L_{SD} = 2$ μm, a gate length $L_G = 220$ nm, and a total gate width $W_G = 2 \times 25$ μm.

III. Results

Following the device fabrication, capacitance-voltage measurements were performed on a surface-passivated test structure with a large gate periphery (L_G =6 μm and W_G = 1 × 50 μm). As shown in Fig. 1(d), the measured CV curve confirms a single-channel operation of the fabricated HEMTs with no secondary channel induced by silicon δ-doping. The two-dimensional electron gas (2DEG) density at different gate biases under the gate was extracted following $n_s = \int_{V_{th}}^{V_{GS}} CdV/(qA)$, where V_{th} is the threshold voltage, q is the magnitude of the electron charge, and A is the area of the Schottky gate contact. The extracted 2DEG density at a zero gate bias is 2.76 × 10^{13} cm^{-2}.

Fig. 2(a) and 2(b) show the logarithmic- and linear-scale transfer characteristics of the fabricated HEMTs, respectively, prior to PECVD SiN passivation. The threshold voltage of the device was −3.95 V, defined as the gate voltage at which the drain current density reaches 1 mA/mm. Unpassivated pHEMTs showed good gate control, demonstrating a 7 orders of on/off ratio and sharp pinch-off characteristics at a drain bias of 10 V. A peak extrinsic transconductance g_m = 0.32 S/mm was measured at the same drain bias. The measured g_m is lower than expected for the 6 nm AlN barrier, which is attributed in part to unoptimized contact resistance. Contact resistance and sheet resistance, extracted using the linear transfer length method, ranged from 0.27 to 0.39 Ω·mm and from 249 to 385 Ω/sq, with the average values of 0.33 Ω·mm and 330 Ω/sq, respectively, as shown in Fig. 2(c). Accordingly, g_m ranged from 0.26 to 0.41 S/mm, with the average value of 0.33 S/mm. Devices after PECVD SiN passivation exhibited a higher off-state gate leakage current density of $I_G \sim 5 \times 10^{-5}$ A/mm. No significant changes in on-state drain current density or transconductance were measured after device passivation. Further optimization of the device passivation process will be needed to minimize the gate leakage current. The output curves in Fig. 2(d) show a maximum drain current density of 1.25 A/mm at a gate voltage V_{GS} = 2 V and repeatable current saturation over a wide range of V_{GS}.

Next, small-signal RF measurements were performed to examine the device speed using GSG probes on surface-passivated two-finger HEMTs. After short-open-load-through calibration, scattering parameters were measured in the frequency range of 100 MHz to 40 GHz, and pad parasitics were de-embedded using on-wafer open and short pads. As shown in Fig. 3(a), the cutoff frequency f_T and maximum oscillation

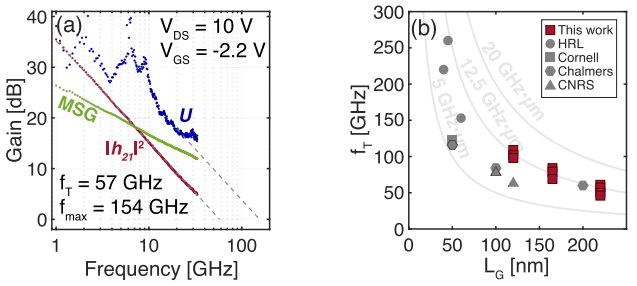

Fig. 3. (a) Small signal characteristics of surface-passivated δ-doped pHEMTs on bulk AlN with a gate length of 220 nm, showing an extracted f_T and f_{max} of 57 GHz and 154 GHz, respectively. (b) Gate length scaling behavior of surface-passivated pHEMTs on AlN (red symbols) from this work along with that of metal-polar GaN DH-HEMTs with a T-gate and surface passivation reported in the literature [14], [20], [21], [22], [23], [24], [25]. Measured devices feature source-to-drain spacing of 2 μm and a device width of 2 $\times$ 25 μm.

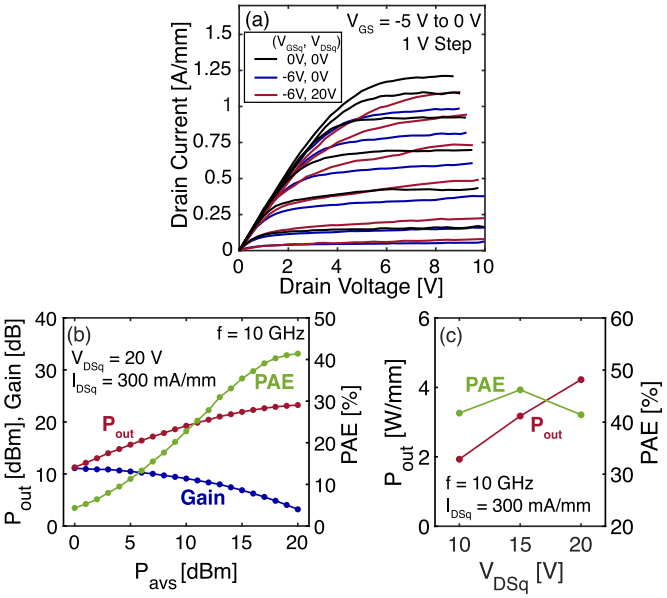

Fig. 4. Pulsed I-V characteristics of surface-passivated δ-doped pHEMTs. (b) Continuous-wave load-pull power sweep at 10 GHz performed on surface-passivated devices, showing P_{out} of 4.2 W/mm and associated PAE of 41.5%. (c) P_{out} and PAE of a pHEMT biased at V_{DSq} = 10, 15, and 20 V, showing a linear increase in P_{out} as a function of V_{DSq}.

frequency f_{max} were estimated to be 57 GHz and 154 GHz, respectively, for a representative 220 nm gate length device biased at the peak g_m condition. To extract f_{max}, the values of U in the frequency range from 20 GHz to 24 GHz were used for extrapolation, following a -20 dB/dec slope. Due to the limited frequency span and noise in U, a broader frequency measurement window will be needed to more accurately determine f_{max}. Upon lateral scaling, the extracted f_T increased to 110 GHz in a device with $L_G = 120$ nm, demonstrating the promise of pHEMTs on single-crystal AlN for high-frequency applications. Fig. 3(b) shows the $1/L_G$ scaling behavior of the pHEMTs on single-crystal AlN with varying L_G and fixed L_{SD} of 2 μm, showing an $f_T \cdot L_G$ product ranging from 10.1 to 13.9 GHz·μm, which is comparable to that of the GaN DH HEMTs reported in the literature. A curve corresponding to 12.5 GHz·μm is shown in Fig. 3(b) to represent the average $f_T \cdot L_G$ value of the pHEMTs.

To investigate the dynamic response of δ-doped pHEMTs, pulsed I-V measurements were carried out using 500 ns long pulses at a 1 ms period. As shown in Fig. 4(a), moderate DC–RF dispersion was observed in surface-passivated devices under a stress bias condition of V_{GSq}, $V_{DSq} = -6$ V, 20 V, compared to the cold bias condition of V_{GSq}, $V_{DSq} = 0$ V, 0 V. The current collapse, evaluated at $V_{GS} = 0$ V, is approximately 15% at the knee voltage. This non-negligible DC-RF dispersion is likely due to the remaining surface traps associated with the PECVD SiN passivation process, which was not optimized for these δ-doped pHEMTs and was performed without any surface pretreatment.

The continuous-wave (CW) large-signal characteristics of the δ-doped pHEMTs were measured. Surface-passivated devices, biased at V_{DSq}, $I_{DSq} = 20$ V, 0.3 A/mm, demonstrated an output power density (P_{out}) of 4.2 W/mm and associated power added efficiency (PAE) of 41.5% at 10 GHz, as shown in Fig. 4(b). Based on the expression for P_{out} of class A amplifiers, $P_{out} = I_{D,knee}(V_{DS,max} - V_{DS,knee})/8$, the dynamic knee current density $I_{D,knee} = 0.96$ A/mm is estimated, which is consistent with the pulsed I-V data shown in Fig. 4(a). The source and load reflection coefficients were $\Gamma_S = 0.04$ - j0.02 and $\Gamma_L = 0.77 + j0.12$, respectively. Due to the source impedance not being conjugate matched, the transducer gain (G_T) at the available power at source $P_{avs} = 0$ dBm was 11 dB, which is lower than the measured power gain (G_P) of 20.5 dB. At $P_{avs} = 20$ dBm, the measured P_{out}, input power (P_{in}), DC drain current, and DC voltage were 23.25 dBm (4.23 W/mm), 10.94 dBm (0.25 W/mm), 0.48 A/mm, and 20.0 V, respectively, yielding a PAE $= (P_{out} - P_{in})/P_{DC}$ of 41.5%. Biasing beyond 20 V is presently limited by device breakdown. Improvements in device design and proper impedance matching are expected to further enhance the large-signal performance. Fig. 4(c) shows P_{out} and PAE of the device measured at different drain biases, showing a linear increase in P_{out}.

IV. Summary

The DC and RF characteristics of silicon δ-doped, pseudomorphic AlN/GaN/AlN HEMTs with PECVD SiN passivation are reported. The as-grown heterostructure exhibits higher electron mobility and lower sheet resistance compared to its undoped counterpart [18]. The fabricated devices demonstrated good gate control and strong potential for mmWave operation, showing, in devices with $L_G = 220$ nm, representative values of $f_T/f_{max} = 57/154$ GHz, P_{out} of 4.2 W/mm and associated PAE of 41.5% under CW operation at 10 GHz. While further device optimization is needed, this initial demonstration of silicon δ-doped pseudomorphic HEMTs on single-crystal AlN substrates provide a promising path toward the development of thermally efficient RF transistors.

Acknowledgment

The authors would like to thank William Harmon and Marty Chumbes for their assistance with the load-pull measurements at RTN.

REFERENCES

[1] M. Micovic, P. Hashimoto, M. Hu, I. MilosavIjevic, J. Duvall, P. J. Willadsen, W. S. Wong, A. M. Conway, A. Kurdoghlian, P. W. Deelman, J.-S. Moon, A. Schmitz, and M. J. Delaney, "GaN double ifeterojunction field effect transistor for microwave and millimeterwave power applications," in *IEDM Tech. Dig.*, Sep. 2004, pp. 807–810.

[2] Y. Tang, K. Shinohara, D. Regan, A. Corrion, D. Brown, J. Wong, A. Schmitz, H. Fung, S. Kim, and M. Micovic, "Ultrahigh-speed GaN high-electron-mobility transistors with f_T/f_{max} of 454/444 GHz," *IEEE Electron Device Lett.*, vol. 36, no. 6, pp. 549–551, 2015.

[3] J. Kotani, J. Yaita, K. Homma, S. Ozaki, A. Yamada, M. Sato, T. Ohki, and N. Nakamura, "24.4 W/mm X-band GaN HEMTs on AlN substrates with the LPCVD-grown high-breakdown-field SiN_X layer," *IEEE J. Electron Devices Soc.*, vol. 11, pp. 101–106, 2023.

[4] W. Liu and A. A. Balandin, "Thermal conduction in $Al_xGa_{1-x}N$ alloys and thin films," *J. Appl. Phys.*, vol. 97, no. 7, Apr. 2005, Art. no. 073710, doi: 10.1063/1.1868876.

[5] L. R. Norman, Z. Abdallah, J. W. Pomeroy, G. Drandova, J. Jimenez, A. Xie, A. Lucero, and M. Kuball, "Impact of AlGaN back barrier on the thermal resistance of RF HEMTs," *IEEE Electron Device Lett.*, vol. 46, no. 7, pp. 1047–1050, Jul. 2025.

[6] R. L. Coffie, *High Power High Frequency Transistors: A Material's Perspective*. Cham, Switzerland: Springer, 2020, pp. 5–41, doi: 10.1007/978-3-030-20208-8_2.

[7] M. Meneghini, C. De Santi, I. Abid, M. Buffolo, M. Cioni, R. A. Khadar, L. Nela, N. Zagni, A. Chini, F. Medjdoub, G. Meneghesso, G. Verzellesi, E. Zanoni, and E. Matioli, "GaN-based power devices: Physics, reliability, and perspectives," *J. Appl. Phys.*, vol. 130, no. 18, Nov. 2021, Art. no. 181101, doi: 10.1063/5.0061354.

[8] H. C. Nochetto, N. R. Jankowski, and A. Bar-Cohen, "The impact of GaN/substrate thermal boundary resistance on a HEMT Device," in *Proc. ASME Int. Mech. Eng. Congr. Expo.*, vol. 10, Nov. 2011, pp. 241–249, doi: 10.1115/IMECE2011-65562.

[9] G. J. Riedel, J. W. Pomeroy, K. P. Hilton, J. O. Maclean, D. J. Wallis, M. J. Uren, T. Martin, U. Forsberg, A. Lundskog, A. Kakanakova-Georgieva, G. Pozina, E. Janzen, R. Lossy, R. Pazirandeh, F. Brunner, J. Wurfl, and M. Kuball, "Reducing thermal resistance of AlGaN/GaN electronic devices using novel nucleation layers," *IEEE Electron Device Lett.*, vol. 30, no. 2, pp. 103–106, Feb. 2009.

[10] G. Li, B. Song, S. Ganguly, M. Zhu, R. Wang, X. Yan, J. Verma, V. Protasenko, H. Grace Xing, and D. Jena, "Two-dimensional electron gases in strained quantum wells for AlN/GaN/AlN double heterostructure field-effect transistors on AlN," *Appl. Phys. Lett.*, vol. 104, no. 19, May 2014, Art. no. 193506, doi: 10.1063/1.4875916.

[11] M. Qi, G. Li, S. Ganguly, P. Zhao, X. Yan, J. Verma, B. Song, M. Zhu, K. Nomoto, H. Xing, and D. Jena, "Strained GaN quantum-well FETs on single crystal bulk AlN substrates," *Appl. Phys. Lett.*, vol. 110, no. 6, Feb. 2017, Art. no. 063501, doi: 10.1063/1.4975702.

[12] A. L. Hickman, R. Chaudhuri, S. J. Bader, K. Nomoto, L. Li, J. C. M. Hwang, H. Grace Xing, and D. Jena, "Next generation electronics on the ultrawide-bandgap aluminum nitride platform," *Semicond. Sci. Technol.*, vol. 36, no. 4, Mar. 2021, Art. no. 044001, doi: 10.1088/1361-6641/abe5fd.

[13] S. Kim, E. Kim, H. Walwil, D. C. Shoemaker, J. Encomendero, M. T. DeJarld, M. B. Tahhan, E. M. Chumbes, J. R. Laroche, D. Jena, H. G. Xing, and S. Choi, "Thermal characterization and design of AlN/GaN/AlN HEMTs on foreign substrates," *IEEE Electron Device Lett.*, vol. 46, no. 5, pp. 817–820, May 2025.

[14] A. Hickman, R. Chaudhuri, L. Li, K. Nomoto, S. J. Bader, J. C. M. Hwang, H. G. Xing, and D. Jena, "First RF power operation of AlN/GaN/AlN HEMTs with >3 A/mm and 3 W/mm at 10 GHz," *IEEE J. Electron Devices Soc.*, vol. 9, pp. 121–124, 2021.

[15] A. Yoshikawa, T. Nagatomi, K. Nagase, S. Sugiyama, and L. J. Schowalter, "Pseudomorphic growth of a thin-GaN layer on the AlN single-crystal substrate using metal organic vapor phase epitaxy," *Jpn. J. Appl. Phys.*, vol. 63, no. 6, Jun. 2024, Art. no. 060903, doi: 10.35848/1347-4065/ad565a.

[16] G. Alvarez-Escalante, R. Page, R. Hu, H. G. Xing, D. Jena, and Z. Tian, "High thermal conductivity and ultrahigh thermal boundary conductance of homoepitaxial AlN thin films," *APL Mater.*, vol. 10, no. 1, Jan. 2022, Art. no. 011115, doi: 10.1063/5.0078155.

[17] Y.-H. Chen, J. Encomendero, C. Savant, V. Protasenko, H. Xing, and D. Jena, "Electron mobility enhancement by electric field engineering of AlN/GaN/AlN quantum-well HEMTs on single-crystal AlN substrates," *Appl. Phys. Lett.*, vol. 124, no. 15, Apr. 2024, Art. no. 152111, doi: 10.1063/5.0190822.

[18] Y.-H. Chen, J. Encomendero, C. Savant, V. Protasenko, H. Xing, and D. Jena, "High conductivity coherently strained quantum well XHEMT heterostructures on AlN substrates with delta doping," *Appl. Phys. Lett.*, vol. 125, no. 14, Sep. 2024, Art. no. 142110, doi: 10.1063/5.0228253.

[19] R. T. Bondokov, S. P. Branagan, N. Ishigami, J. Grandusky, T. Nagatomi, K. Tatsuta, T. Miebach, and J. Chen, "Two-inch aluminum nitride (AIN) single crystal growth for commercial applications," *ECS Meeting Abstr.*, vol. MA2021-02, no. 34, p. 985, Oct. 2021, doi: 10.1149/ma2021-0234985mtgabs.

[20] R. Kabouche, J. Derluyn, R. Pusche, S. Degroote, M. Germain, R. Pecheux, E. Okada, M. Zegaoui, and F. Medjdoub, "Comparison of C-doped AlN/GaN HEMTs and AlN/GaN/AlGaN double heterostructure for mmW applications," in *Proc. 13th Eur. Microw. Integr. Circuits Conf. (EuMIC)*, Sep. 2018, pp. 5–8.

[21] G. Meneghesso, M. Meneghini, F. Medjdoub, Y. Tagro, B. Grimbert, D. Ducatteau, N. Rolland, R. Silvestri, and E. Zanoni, "First reliability demonstration of sub-200-nm AlN/GaN-on-silicon double-heterostructure HEMTs for Ka-band applications," *IEEE Trans. Device Mater. Rel.*, vol. 13, no. 4, pp. 480–488, Dec. 2013.

[22] K. Shinohara, A. Corrion, D. Regan, I. Milosavljevic, D. Brown, S. Burnham, P. J. Willadsen, C. Butler, A. Schmitz, D. Wheeler, A. Fung, and M. Micovic, "220 GHz f_T and 400 GHz f_{max} in 40-nm GaN DH-HEMTs with re-grown ohmic," in *IEDM Tech. Dig.*, Dec. 2010, pp. 30.1.1–30.1.4.

[23] K. Shinohara, D. Regan, I. Milosavljevic, A. L. Corrion, D. F. Brown, P. J. Willadsen, C. Butler, A. Schmitz, S. Kim, V. Lee, A. Ohoka, P. M. Asbeck, and M. Micovic, "Electron velocity enhancement in laterally scaled GaN DH-HEMTs with f_T of 260 GHz," *IEEE Electron Device Lett.*, vol. 32, no. 8, pp. 1074–1076, Aug. 2011.

[24] K. Shinohara, I. Milosavljevic, S. Burnham, A. Corrion, P. Hashimoto, D. Wong, M. Hu, C. Butler, A. Schmitz, P. J. Willadsen, K. S. Boutros, H. Kazemi, and M. Micovic, "60-nm GaN/AlGaN DH-HEMTs with 1.0 Ω·mm R_{on}, 2.0 A/mm I_{dmax}, and 153 GHz f_T," in *Proc. Device Res. Conf.*, Jun. 2009, pp. 167–168.

[25] A. Malmros, P. Gamarra, M. Thorsell, H. Hjelmgren, C. Lacam, S. L. Delage, H. Zirath, and N. Rorsman, "Impact of channel thickness on the large-signal performance in InAlGaN/AlN/GaN HEMTs with an AlGaN back barrier," *IEEE Trans. Electron Devices*, vol. 66, no. 1, pp. 364–371, Jan. 2019.